Microstructural investigation of slag-blended UHPC: The effects of slag content and chemical/thermal activation

Omar Abdulkareem, Amor Ben Fraj, Marwen Bouasker, Lahcen Khouchaf, Abdelhafid Khelidj

Microstructural investigation of slag-blended UHPC: The effects of slag content and chemical/thermal activation

Omar M. Abdulkareem[a,b,c], Amor Ben Fraj[a,*], Marwen Bouasker[d], Lahcen Khouchaf[e], Abdelhafid Khelidj[b]

[a]*Cerema, Project Team DIMA, 120 rue de Paris, BP 216 Sourdun, 77487 Provins Cedex, France*

[b]*University of Nantes, IUT Saint-Nazaire, GeM, UMR CNRS 6183, 58 rue Michel Ange, BP 420-44600, Saint-Nazaire, France*

[c]*University of Mosul, College of Engineering, Department of Environmental Engineering, 41002 Mosul, Iraq*

[d]*Université d'Orléans, Université de Tours, INSA Centre Val de Loire, Laboratoire de Mécanique Babriel Lamé (LaMé), Polytech Orléans, 8 rue Léonard de Vinci, 45072 Orléans, France*

[e]*IMT Lille Douai, Lille Université, Cité Scientifique, Rue Guglielmo Marconi, BP 20145, 59653 Villeneuve d'Ascq Cedex, France*

ABSTRACT

This paper focuses on the microstructural investigation of ultra-high performance concrete (UHPC) mixtures featuring various replacement levels for blast furnace slag (BFS), in the aim of becoming more environmentally-friendly. Three levels of slag are applied (namely 30%, 50% and 80%) per unit volume of cement. The microstructural characteristics examined included X-ray diffraction (XRD) analysis, transmission electron microscopy (TEM), and mercury intrusion porosimetry (MIP). These characteristics are assessed along with the mechanical strengths at 3 and 90 days. Similarly, the effects of chemical and thermal activation methods on incorporating BFS into UHPC mixtures at high volumes were studied from a microstructural point of view, and a comparison is drawn between the non-activated and activated mixtures.

The results of this investigation show that the beneficial physical impact of slag replacement lies at the 30% level, due to its filler property in stimulating hydration to quickly generate portlandite. For this reason, the portlandite and C-S-H peaks are quite similar to those in the reference mixture (i.e. 0% BFS) at 3 and 90 days, as demonstrated in the XRD analysis. Moreover, the pore size distribution could be refined, the microstructure densified (as indicated on the TEM images), and compressive strengths at both ages improved. In contrast, for slag replacement levels of 50% and 80%, the portlandite and C-S-H peaks are significantly lowered, as observed in the XRD analysis, thus causing a magnification of the capillary pores

*Corresponding author. Address: Cerema Île-de-France, 120 rue de Paris, 77171 Sourdun, France
Phone: +33 1 60 52 33 62
email address: **amor.ben-fraj@cerema.fr** (A. Ben Fraj)

and a drop in compressive strength at 3 and 90 days. Chemical activation through a potassium hydroxide, with a dosage of 10.17 kg/m^3, at the 80% BFS replacement level is able to accelerate hydration and portlandite consumption, as exhibited in the XRD analysis through the absence of portlandite peaks and limited quantities of C-S-H at 3 and 90 days. However, this step results in smaller pores and a higher compressive strength. As for the thermal activation, the portlandite in the blended mixtures with 50% and 80% BFS replacement decreases in quantity, as confirmed by XRD analysis, and the reaction is perfectly activated by means of the solubility acceleration of the alkalis; consequently, the pore structure is compacted, as revealed on the TEM image and the compressive strength rises considerably.

Keywords: Ultra-High Performance Concrete (UHPC), Blast Furnace Slag (BFS), Chemical Activation, Thermal Activation, Microstructure, XRD, TEM, MIP.

1. Introduction and scientific background

Ultra-high performance concrete (UHPC) was developed during the 1990's. Richard and Cheyrezy [1] introduced the primary formulation, in which they excluded coarse aggregate in order to increase homogeneity and avoid weakening the microstructure simultaneously given that the bond between coarse aggregate and cement paste is the most fragile in the system. This formulation thus leads to a more efficient UHPC, whose strength and durability is primarily ascribed to a highly compact composite matrix with practically no capillaries (i.e. minimal porosity). More specifically, the material's porosity is continuous [2, 3] since the UHPC mix design relies on both a tight packing density and the use of additional cementing materials, such as silica fume, for the purpose of filling voids between larger particles, thus enhancing the flow characteristics and promoting minor C-S-H generation [4, 5]. Courtial *et al.* [3] revealed images, by means of a scanning electron micrograph, of the perfectly homogeneous UHPC matrix through exposing widespread anhydrous cement (appearing in light gray), hydrate compounds (medium gray), a perfect dispersion of silica fume due to the polycarboxylate superplasticizer effect, and perfect filling of the Interface Transition Zone (ITZ) by hydrates emerging from the pozzolanic reaction of silica fume. Moreover, the crushed quartz distribution is homogeneous everywhere in the UHPC paste. Tam *et al.* [6] indicated that the minimal water amount present in UHPC inhibits the dissolution of silica fume in the pozzolanic reaction between portlandite and silica fume, hence the reaction is not complete. This finding has been emphasized by the SEM analysis, which detected several sound spherical particles of silica fume. The particles of both unhydrated cement and silica

fume do indeed play a filling role and participate in further densifying the system. In addition, the existing small amount of water may facilitate the generation of a limited portlandite content, as required for the pozzolanic reaction and generation of new C-S-H, which serves to increase strength. Given that the compressive strength of UHPC lies around 150-200 MPa without any subsequent treatment, the collateral effect of hydration on porosity is as follows: with a rather low w/c ratio, the capillary porosity declines and the ITZ is filled with C-S-H hydrates generated by the pozzolanic reaction of silica fume [3]. Cheyrezy *et al.* found that the cumulative porosity ranged from 3.75 nm to 100 µm and did not exceed 9% for the different UHPC mix designs subjected to various curing methods. The reduction obtained in cumulative porosity is corroborated by a lowering of the threshold value, whereas for other mixtures, the threshold value remains quite small and cannot be derived by mercury intrusion; hence, cumulative porosity is neglected. Furthermore, Cheyrezy *et al.* [7] observed, through an XRD experiment conducted on various UHPC mixtures, the appearance of C_3S and C_2S peaks for unhydrated cement, even for specimens cured at high temperature, while the portlandite peak cannot be distinguished for the UHPC specimens cured at temperatures above 200ºC. This finding underscores the activation of the pozzolanic reaction with temperature. The highly compact skeleton in the hardened UHPC paste with a small number of air pores can be recognized in the SEM images. The major hydration product is C-S-H gel, which features an identical morphology, whereas both portlandite and ettringite are absent [8, 9]. Maroliya [10] found, through the XRD patterns of UHPFRC mixtures, that both portlandite and SiO_2 are considered as the main phases for entire mixtures, in addition to the increased portlandite intensity and loss of C-S-H in UHPC. The portlandite intensity in a water-cured UHPC specimen at 1 day was greater than that of the heat-cured specimens at 7 days due to the fact that the portlandite content was proportional to the creative degree of C-S-H. Also, both the C_3S and C_2S peak characteristics of unhydrated cement are revealed, even under thermal curing. Oertel *et al.* [11] confirmed, by way of SEM images, that alite particles strictly possess ridged rims in the UHPC paste, and these may serve as dissolution indicators. Moreover, the matrix between clinker particles appears to be even more compact in this paste. It is therefore impossible to distinguish hydration products (e.g. portlandite and C-S-H phases) through morphology or chemical composition. Silica fume particles appear as dark gray spheres. In contrast, Cwirzen *et al.* [12] did not remark any distinct dissimilarity when comparing the pore structure of thermally treated and non-thermally treated UHPC specimens through SEM analysis due to the lack of larger silica fume agglomerates or major quantities of portlandite. The pore structure was more highly densified as a result of the heat treatment

given that a large number of pores were smaller than 10 nm and moreover the pore size distribution did not denote an ITZ presence, which was confirmed by the detection of considerable residual (anhydrous) cement or additional portlandite close to the aggregate particles.

Nonetheless, one downside of UHPC, when manufactured in accordance with existing technology, is the use of a cement quantity that far exceeds ordinary concrete. Based on an evaluation of the reviews spanning the last 10 years, it was found that the mean cement quantity equals nearly 750 kg/m^3 and when whole reactive elements are included, the binder amount reached 925 kg/m^3 [13]. Furthermore, attention is always being focused on CO_2 releases in the manufacturing of cement and concrete, in particular beyond the Kyoto Protocol and Paris Agreement. Because cement manufacturing operations release some 1.6 billion tons of CO_2 annually [14], many studies have sought to modify UHPC by incorporation with cementitious blends (silica fume, fly ash and blast furnace slag) in order to meet numerous technical performance requirements, in addition to sustainability performance criteria for low-emissions concrete manufacturing.

Blast furnace slag (BFS), an industrial byproduct from iron manufacturing, is in abundant supply in both silica and alumina phases [15]. It has been established that BFS, on account of its hydraulic behavior, reacts with water and generates C-S-H [16]. In general, hydrated Portland cement generates portlandite (highly soluble mineral) at around 15% to 25 % (by mass), which can raise the level of porosity, weaken the aggregate/paste bond and hence reduce durability. In contrast, the relative C-S-H content in the cement blended with slag increases and portlandite decreases. The beneficial physical impacts of slag incorporation include: i) a dilution of lime-containing Portland cement compounds (equivalent to an incremental rise in the w/c ratio and inversely correlated with the slag substitution rate); ii) a filler effect due to fine slag particles being inserted between disconnecting cement particles, thus dispersing the reactive particles; and iii) stimulation tied to fine slag particles being represented as nucleation sites for portlandite, hence quickening the dissolution mechanism and both stimulating and inducing cement hydration. Moreover, the chemical impact of slag incorporation includes the reaction of portlandite released from Portland cement with the glass phase of the cement blended with slag. Consequently, the pore structure becomes further refined by decreasing pore size and cumulative pore volume, reinforcing the aggregate/paste interface and enhancing strength and durability [17-19].

Nevertheless, even though BFS can be activated by portlandite and gypsum, the BFS hydration rate in concrete is low, which limits the strength gain and forms a highly compact

UHPC microstructure by decreasing total pore volume and pore linkage while proceeding with perfect filling of the pores in the ITZ [16, 20]. Zhou *et al.* [21] observed that the longer the curing age of the blended slag cement mixtures, the smaller the capillary pore content and size. Furthermore, the gel pore content expands during the first 7 days, and thereafter their size shrinks. Likewise, when the slag replacement level falls below 70%, the greater slag amount results in a finer pore structure, which leads to the blocked structure observed in SEM images, as well as in a compact C-S-H at the later age. As for slag replacement levels exceeding 70%, the microstructure turns highly porous, accompanied by an increased amount of slag. Ca-rich C-S-H is fibrillar in its origin and gradually modifies into a foil-like morphology as the quantity of slag rises [22]. Hadj-Sadok *et al.* [23] reported that the pore size distribution of blended slag mixtures is coarser than that of a conventional mixture at 28 days. The threshold pore access diameter and the average pore radius are both greater in the mixtures containing 30% and 50% slag than in the conventional mixture. Conversely, the pore size distribution of blended slag mixtures tends to develop toward being smaller and finer, as compared to the pores of a conventional mixture at 90 days. Based on XRD results, the following phases exist in cement and slag blends: portlandite, calcite, C-S-H, ettringite, monosulfoaluminate, C_2S, C_3S, C_3A, C_4AF [24]. Schuldyakov *et al.* [25] also noticed a very high content of portlandite through an XRD analysis of the blended mixture with a slag content of up to 70%. In contrast, they observed that the major reflection of β-C_2S was nearly absent when 30% of the slag is replaced in the blended matrix at 28 days. Additionally, XRD analysis confirms the growth of low-basic hydrated calcium silicate in the blended binder, hence the increased slag content in X-ray patterns leads to intensified reflections in the narrow-angle field.

Accordingly, many researchers have attempted to activate the slag in the blended cement either chemically primarily by alkalis or thermally at a specific high temperature and duration, due to its low reactivity at early age coupled with a latent reaction [18, 26]. The porosity, pore size distribution and pore connectivity of alkali-activated slag (AAS) concrete can strongly affect the mechanical strength and durability of the chemically-activated mixture [27]. The microstructural evolution of hydrating AAS mixtures is controlled through quick alterations at the early age and slow evolution later on [28]. Aydin *et al.* [29] observed that NaOH-activated slag concrete has a coarser pore size distribution and many more macro and meso pores than those in water glass-activated slag concrete. The major reaction product of AAS mixture, which cannot be counted on the silica modulus (SiO_2/Na_2O) MS, is the Na-integrated C-S-H. This observation was confirmed by Shi *et al.*[30], who found by XRD analysis that the major

hydration product of the various alkali-activated slag mixtures is C-S-H (with its high peak denoting greater C-S-H crystallinity in the AAS structure), whereas the secondary hydration products vary with the type of activator. A slight divergence can be detected however between NaOH- and KOH-activated slags. The C-S-H crystallinity in NaOH-activated slag cement is clearly greater than that in water glass-activated slag cement. As noticed through SEM images, NaOH-activated slag cement contains a diffuse reaction ring around the hydrating slag particles, in addition to exhibiting a diffusion-controlled reaction [31].

Abd-El Aziz *et al.* [32] indicated that the slag reactivity increases with curing temperature, thus leading to a rise in the portlandite consumption rate via the pozzolanic reaction and the generation of further hydration products. This results in raising the chemically bound water and reducing total pore size with curing temperature for all blended mixtures. However, this water diminishes as the curing temperatures rises from 75° to 100ºC by means of converting the initially produced C-S-H with a greater bound water amount to C-S-H containing just a small amount of bound water. Moreover, Aldea *et al.* [33] confirmed through XRD the absence of any obvious tendency to generate portlandite content in the blended mixtures with either autoclave-cured or steam-cured slag.

This study proposes bridging the existing knowledge gap by performing detailed studies on microstructural measurements of eco-friendly UHPC specimens as a function of cement replacement rate by BFS. These measurements comprise XRD, TEM and MIP. Similarly, this study presents an overview of the mechanical properties linked with the microstructural development of blended mixtures. Moreover, investigations deal with the effect of chemical and thermal activation of high BFS replacement rates contained in UHPC mixtures. Comparisons are drawn from a microstructural perspective between the activated and reference UHPC. The goal herein is to detect the influence of each activation process on the modification of assembly and pore development phases in conjunction with mechanical strength.

2. Experimental program

2.1 Materials and mixtures

The components of the reference-binder phase of UHPC mixture studied here include a Type I ordinary portland cement (C) from Le Teil, Silica Fume (SF) from Condensil and Crushed Quartz (CQ) from Sibelco. For other UHPC mixtures, cement is vol. substituted with ground granulated blast furnace slag (BFS) from Ecocem. The chemical composition of different components and their physical properties are given in Table 1.

Figure 1 depicts the X-Ray patterns of cement, Blast Furnace Slag and Gray (silicium) Silica Fume. The XRD patterns of BFS and SF mainly reveal an amorphous nature [34]. The vitreous aspect of BFS is clearly illustrated by a large halo on the XRD pattern.

Table 1: Chemical composition and physical properties of different components

	Component	Cement	Silica Fume	Blast-Furnace-Slag	Crushed Quartz	Quartz Sand
Components' identification	Trade name	CEM I 52.5 SR5	S95 B DM	-	C500	CV32
	Plant	Le Teil	Condensil	Ecocem	Sibelco	Sibelco
	Abbreviation	C	SF	BFS	CQ	QS
Chemical composition (% mass)	CaO	65.00	0.30	43.90	<0.03	0.01
	SiO_2	22.00	95.00	37.40	>99.1	>99.00
	Al_2O_3	2.78	-	10.90	<0.46	0.49
	Fe_2O_3	2.42	-	0.70	<0.05	0.03
	K_2O	0.17	-	0.24	<0.31	0.35
	MgO	0.76	-	6.50	-	-
	Na_2O_{eq}	0.24	0.08	0.46	-	-
	SO_3	2.20	0.06	0.10	-	-
	MnO	0.01	-	-	-	-
	TiO_2	0.17	-	0.50	<0.02	0.02
	Cl^-	<0.10	0.10	0.01	-	-
	S^{2-}	<0.10	-	0.80	-	-
	LOI	0.90	0.60	<1.5	-	-
Physical properties	SS (cm^2/g)	3555*	250000**	4450*	10435*	124*
	Density	3.17	2.24	2.9	2.65	2.65

*Blaine method; **BET method

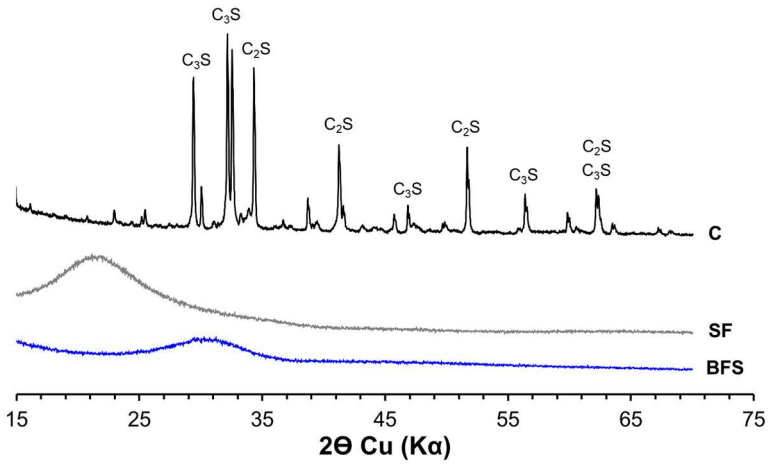

Figure 1. X-ray diffraction (XRD) patterns of used materials

Figure 2 shows a slag particle containing metallic fibers, which are attributed to the iron manufacturing origin of BFS. The EDS analysis (Fig. 3) of this particle confirms the presence

of metal components. According to Figure 3, the slag particle contains aluminum, silicon, iron and carbon elements in a disordered combination along with oxygen, which agrees with the chemical composition provided of the slag used herein. The copper stems from the sample carrier. Generally speaking, the chemical composition of slag influences its reactivity, which intensifies with increases in alkalinity and in calcium, alumina and magnesium amounts, as well as with lower silica and magnesia amounts [**35**].

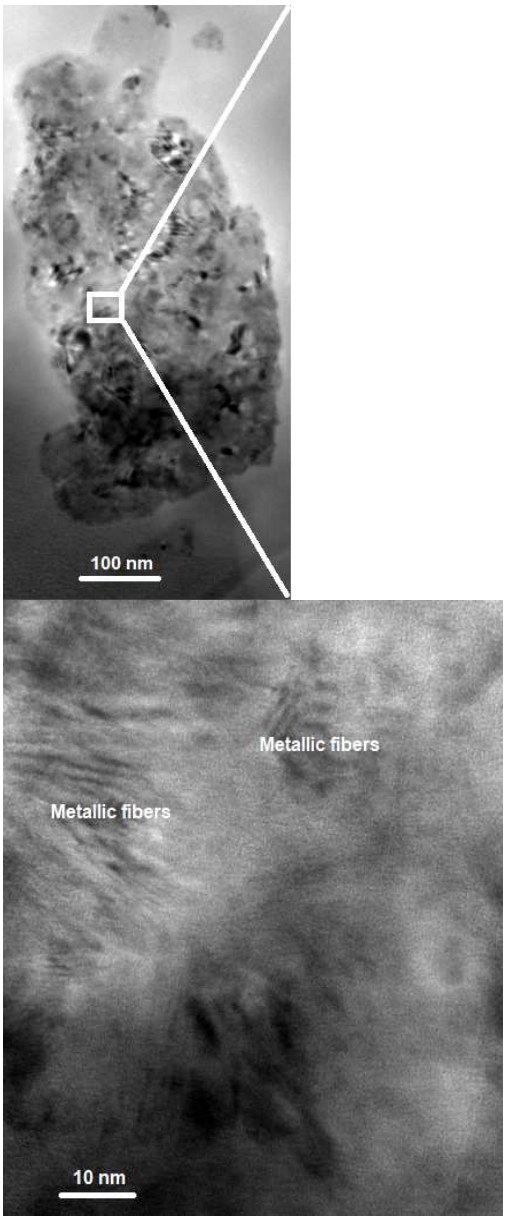

Figure 2. TEM image of a slag particle

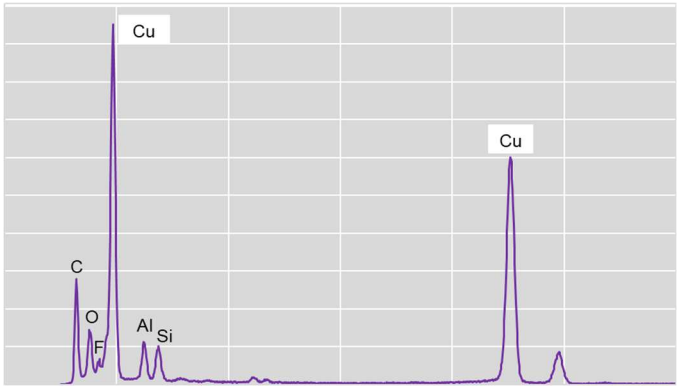

Figure 3. EDS analysis of a slag particle

To ensure the self-compactness of manufactured UHPC, a polycarboxylate Sika Viscocrete Krono HE 20 superplasticizer (SP) has been added. This additive is known as a high water reducer with a density and solid content of 1.085 and 41%, respectively. The content of this acrylic copolymer was adjusted to ensure the same slump flow for all UHPC mixtures regardless of their BFS content. All mix designs feature the same water-to-binder content (in considering the water provided by the superplasticizer). The optimization of these concrete mixtures has been detailed in [34]. A 15-L mixer, with high energy (Eirich intensive mixer) is used. It has a star-blade, tilted drum, and high mixing speed of up to 40 m/s (opposed currents). This results in optimum dispersion of particles, and high mixture homogenization with low mixing time (3 minutes).

Table 2 summarizes the studied UHPC mixtures and their physico-chemical properties. Our objective is to compare different mixtures, with the same water-to-binder ratio (0.14), the same slump flow (300 mm), and with different contents of BFS.

Even if the slump flow is the same for all studied mixtures, the maximum reaction heat and temperature measured in semi-adiabatic conditions decrease with increasing BFS content. The initial setting time is accelerated by the nucleation effect of low BFS content ($UHPC_2$), and delayed with high BFS content, denoting a dilution effect.

Table 2: Composition and physico-chemical properties of the studied UHPC mixtures

Components (kg/m³)	**$UHPC_1$**	**$UHPC_2$**	**$UHPC_3$**	**$UHPC_4$**	**$UHPC_5$**
C	977.0	683.9	488.5	195.4	195.4
SF	183.0	183.0	183.0	183.0	183.0
CQ	61.0	61.0	61.0	61.0	61.0
BFS	-	268.1	446.9	715.0	715.0
QS	1075.0	1075.0	1075.0	1075.0	1075.0
SP	25.31	10.54	22.49	25.31	25.31
W	145.63	160.39	148.44	145.63	145.63
KOH	-	-	-	-	10.17
Physico-chemical properties [34, 36]					
Slump flow (mm)			300		
Maximum heat, q_{max} (J/g)	161	159	132	91	91

Temperature, T_{max} (°C)	67.4	66.5	54.1	37.2	41.4
Initial setting time (min)	330	150	450	750	660

Immediately after mixing, concrete is poured into prismatic 40×40×160 mm^3 steel molds and stored for 24 h before demolding and plastic wrapping, to avoid any drying. Subsequently, the specimens were stored in a fog room at 20ºC for 3 and 90 days, except for thermally activated mixture.

2.2 Methods

- *Chemical/thermal activation*

In order to compensate for the lack of alkalis when cement is substituted with BFS, KOH is added, particularly for high BFS content. This results in improving the compressive strength at early age. In this study, we will focus on $UHPC_5$, for which 80% of cement is replaced by BFS, and activated by 10.17 kg/m^3 of KOH. The optimization of hydroxide potassium concentration is detailed in [34]. To maintain the same slump flow, additional 30 s of mixing time are necessary for chemically activated mixture.

Thermal activation is employed to accelerate concrete maturity at a given equivalent age. For this study, thermal activation is notably applied on concretes with a high BFS content ($UHPC_3$ and $UHPC_4$) in order to ensure the same long-term properties as $UHPC_1$. The equivalent age should therefore be more than 90 days. The optimization of activation temperature and duration is detailed in [36].

- *X-ray diffraction*

A Bruker D8 X-ray diffractometer in a θ-2θ configuration with an incident beam monochromator and CuKα radiation (λ = 1.54Å) operating at a generator voltage of 40 kV and current of 30 mA has been used. The XRD analysis was performed at 3 and 90 days. The UHPC specimen was crushed in a percussion crusher and afterwards placed in an agate mixture. A surplus of ethanol was added (to prevent further hydration of the cement and support grinding), and the mixture was ground by hand to a fine powder (< 63 µm).

- *Transmission electron micrography*

The radiation experiment (scanning) on the specimens and chemical analysis were carried out using a Transmission Electron Micrograph FEI Tecnai G2-20, operated at a 200-kV accelerating potential. The device was equipped with a filament of lanthanum hexaboride

LaB6, a double tilt holder and a Gatan digital camera. For BFS particle, the analysis was performed with an EDAX/EDX spectrometer.

- *Pore size distribution*

The porosity and pore size distribution were determined by means of Mercury Intrusion Porosity (MIP) using an Autopore IV porosimeter. This test was conducted on 1-cm^3 specimens at both 3 and 90 days. At 3 days, the specimens were immersed in methanol so as to block hydration reaction progress before drying at 105°C and testing **[36]**. Every total porosity value represents the average of two measurements.

- *Mechanical properties*

The compressive strength test was carried out on 40 × 40 × 160 mm^3 prismatic specimens at 3 and 90 days, according to NF EN 196-1 [37]. A 300-kN press machine is used, with loading speeds of 2.5 kN/s for the compressive tests. Every strength value represents the average of six specimen strength readings.

3. Results and discussion

3.1 X-ray diffraction

Figure 4 shows the XRD patterns of various UHPC specimens at 3 days. As observed, the quartz (Q) peaks are of similar intensities across all tested UHPCs since they feature the same contents of crushed quartz and quartz sand. After 3 days of hydration, the portlandite (P) content is low and no trace can be found of belite (C_2S).

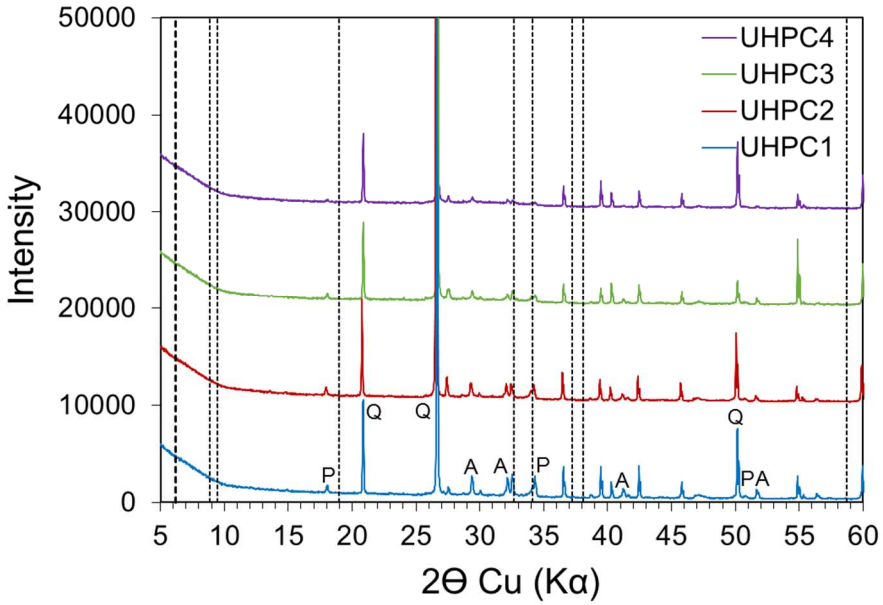

Figure 4. X-ray diffractograms of UHPC mixtures at 3 days (Q=Quartz, P=Portlandite, A=Alite, Hidden line=C-S-H)

The portlandite intensities are practically the same for both $UHPC_1$ and $UHPC_2$, but the incremental BFS amount in both $UHPC_3$ and $UHPC_4$ decreased and their respective peaks dropped. The hydration acceleration of $UHPC_2$ in the presence of 30% BFS [38,34] actually induces an acceleration of portlandite production that is counterbalanced by its rapid consumption by the silica fume. For high BFS contents, the quantity of portlandite produced decreases, and its consumption by the pozzolanic reaction of silica fume increases [39,40], resulting in very small quantities of portlandite even after 3 days of hydration [36]. This portlandite reacts with SF to produce C-S-H [41]; their amorphous nature had led to the emergence of obvious peaks at 32.65°, 34.1° and 60.2° in all patterns. As shown in Figure 4, C-S-H intensities are higher in $UHPC_1$ and gradually diminish as BFS content increases. The C-S-H peaks are particularly low for $UHPC_4$.

Moreover, Figure 4 indicates some unhydrated calcium silicates (C_3S) at 3 days. Unreacted alite is more prominent in $UHPC_1$ than the other blended UHPC mixtures and decreases with greater slag content.

Figure 5 exhibits a reduction in portlandite and alite amounts at 90 days through a weak reflection of peaks compared to that at 3 days. The portlandite is being consumed by the pozzolanic reaction of SF and BFS, which continues at the later ages. The alite reflects continuity in the cement hydration reaction and then a decrease in the amount of unreacted particles. The low cement content of $UHPC_4$ explains the absence of an alite peak at 90 days as well as the lack of portlandite content, which results in a drop in the C-S-H produced. It is also observed that the C-S-H peaks in all UHPC mixtures at 90 days slightly exceed those at 3 days, indicating progression of the hydration phenomenon over the long term and growth in C-S-H to the detriment of portlandite due to the pozzolanic [39] and latent hydraulic reactions of BFS.

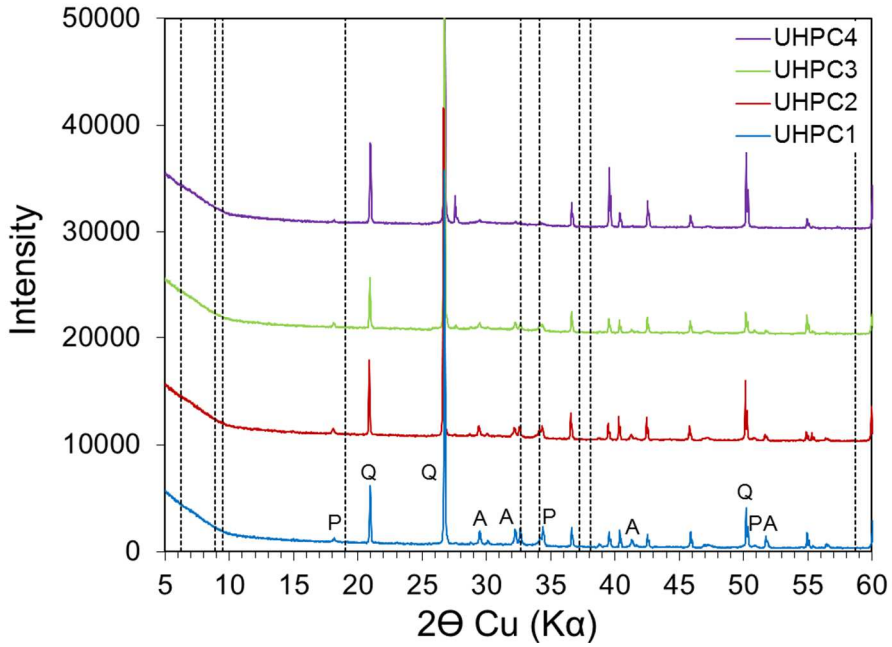

Figure 5. X-ray diffractograms of UHPC mixtures at 90 days (Q=Quartz, P=Portlandite, A=Alite, Hidden line=C-S-H)

Figure 6 shows the influence of chemical activation by KOH through XRD patterns on $UHPC_4$ at both 3 and 90 days. It is obvious that adding KOH solution to the 80% slag in $UHPC_5$ leads to an absence of portlandite at 3 and 90 days [36]. As for $UHPC_4$, the speed of free portlandite release from cement hydration does not offset its consumption by the pozzolanic reaction of silica fume and slag. Moreover, the addition of chemical activator promotes BFS reactivity, which results in an increase of its portlandite consumption. The greater low contents of portlandite and C-S-H imply that the progress of $UHPC_5$ hydration at 90 days might be restricted. The lower reflection peak of $UHPC_5$ at 90 days is correlated with the interrupted release of portlandite from the alite and belite hydration phases, which also become rather limited at this age.

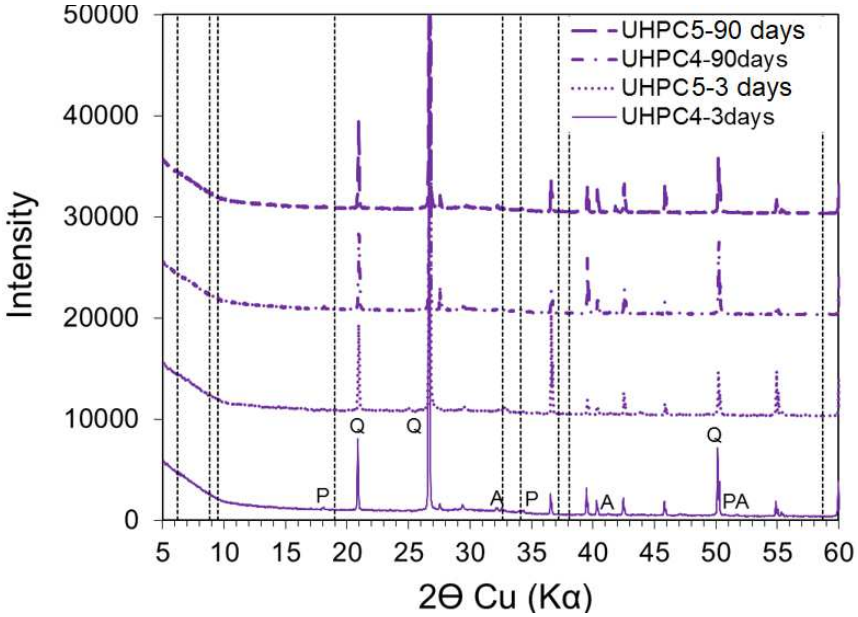

Figure 6. X-ray diffractograms of UHPC$_4$ mixtures with and without chemical activation (Q=Quartz, P=Portlandite, A=Alite, Hidden line=C-S-H)

337

338 From Figure 7, it can be observed that the effect of thermal activation through XRD traces is
339 quite obvious for both UHPC$_3$ and UHPC$_4$. The major phases specified for hydrated cement
340 are: C-S-H gel, unhydrated C_3S, and portlandite. Let's note that the intensities of the
341 diffraction lines of quartz and C_3S increased with the thermal treatment of UHPC$_3$ and
342 UHPC$_4$. In contrast, the intensities of the diffraction lines corresponding to portlandite of both
343 thermally-activated mixtures located at 18° (4.921 Å), 34.1° (2.627 Å) and 50.8° (1.796 Å)
344 are lower than those of the non-activated mixtures. The similar XRD patterns of activated and
345 non-activated mixtures at 90 days highlight the efficiency of the selected temperature and
346 duration for boosting UHPC hydration with high BFS content. It is well known that a hotter
347 temperature helps speed cement hydration and promote the secondary hydration between
348 cementitious materials and portlandite. For BFS, the prime reaction is enhanced by
349 temperature, in the aim of increasing the solubility of alkali hydroxides and releasing
350 considerable portlandite through the cement hydration. In contrast, the quantity of portlandite
351 generated by cement hydration offsets its consumption by slag at advanced ages. For UHPC$_4$-
352 T, consumption prevails over generation and the lower portlandite peaks become more
353 noticeable.

354

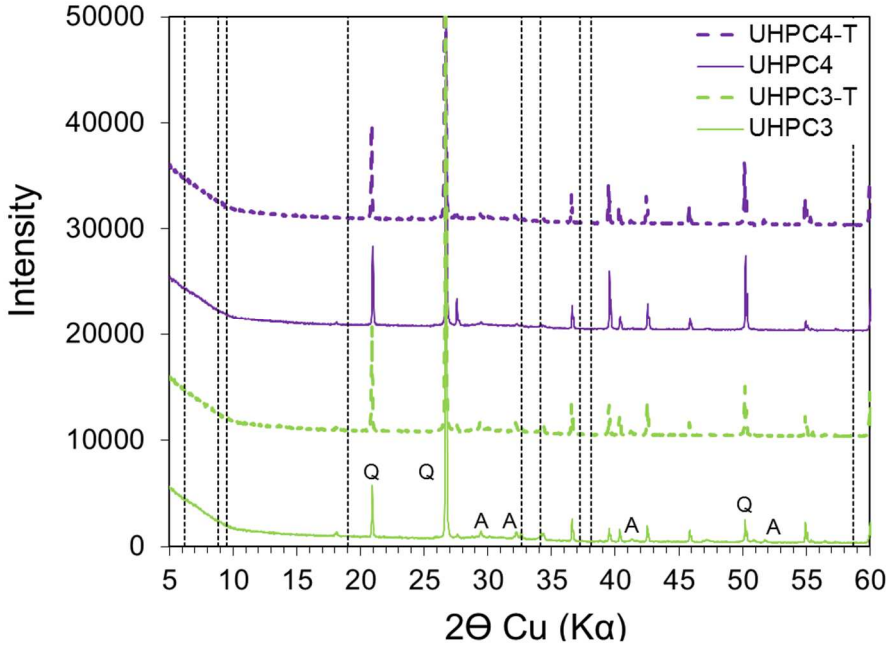

Figure 7. X-ray diffractograms of $UHPC_3$ and $UHPC_4$ mixtures with and without thermal activation (Q=Quartz, P=Portlandite, A=Alite, Hidden line=C-S-H)

3.2 TEM observations

The high resolution of the transmission electron microscopy technique should provide valuable information on the phases formed and their interactions, which depend on: i) BFS content, ii) age of hydration, and iii) applied activation.

Figure 8 displays the somewhat dense internal structure of $UHPC_1$, with perfect quartz particles/hydrated paste interfaces. The quartz particles have an angular shape with a sharp border, while silica fume particles possess different morphological features appearing as light gray spheres with different volumes. The interface between silica fume particles and the matrix is hard to distinguish and appears as cloudy, thus denoting that some hydration reactions occur on the silica fume surface. The hydrated products appear as light gray assemblages, developed on the surface of silica fume particles, as shown in Figure 8; this phenomenon is known as heterogeneous nucleation [**34**]. Figure 9 shows that after 90 days, the hydrates formed accumulate on the silica fume particle surface due to their ultra fineness [**6,42**]. These particles partially reacted with portlandite, which explains the disappearance of a portion from the spherical silica fume.

In Figure 10, the pore structure of $UHPC_1$ appears very dense with a good bond between aggregates and cement matrix. A good dispersion of silica fume can also be noticed, thus confirming the beneficial effect of superplasticizer on UHPC homogeneity [**3**]. The piecemeal dissolution of silica fume and its reaction with portlandite generate new C-S-H hydrates. The

additional C-S-H gel produced in the paste occupies large spaces and reinforces interconnection of the blended mixture; consequently, $UHPC_1$ becomes highly densified and impenetrable [6]. The C-S-H gel hydration products formed on the silica fume particle surface are irregularly shaped, and their presence points to silicon and calcium as major components [39].

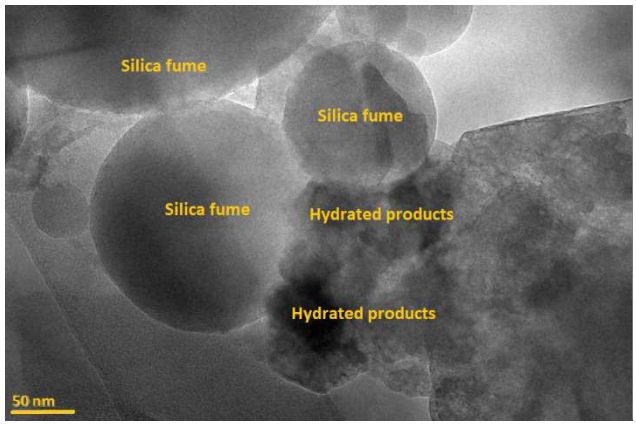

Figure 8. TEM image of $UHPC_1$ at 90 days, showing the heterogeneous nucleation

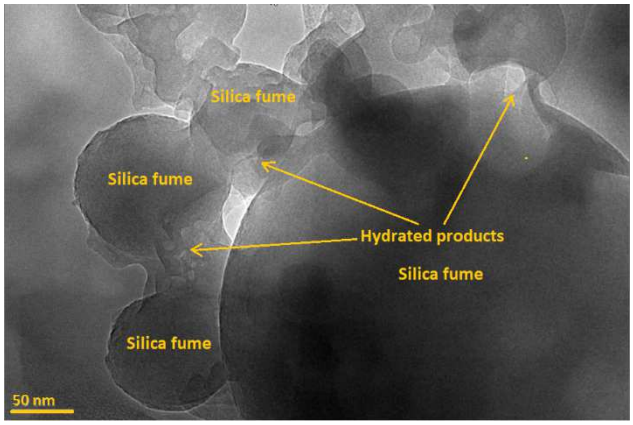

Figure 9. TEM image of $UHPC_1$ at 90 days, showing the partial reaction of silica fume

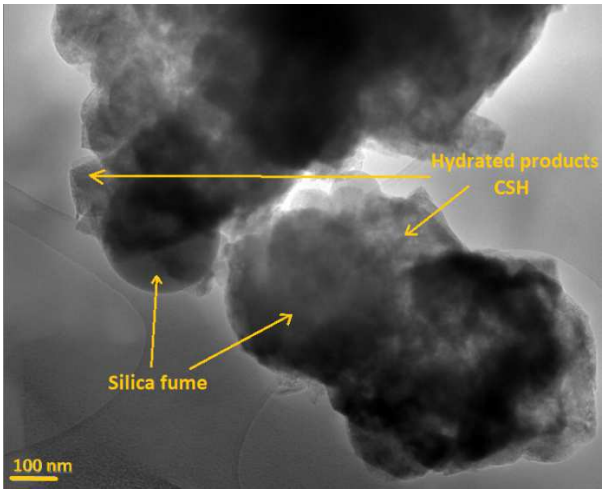

Figure 10. TEM image of $UHPC_1$ at 90 days, showing the hydrated products (C-S-H)

Incorporating 30% slag in $UHPC_2$ achieves high compactness in its microstructure and a pronounced decrease in capillary porosity. As shown in Figure 11, the densified microstructure of $UHPC_2$ at 90 days with little porosity can be represented as extra fine pores by white points, indicating the presence of a refined pore structure. The composite binder particles are closed to one another because of a minimal w/b ratio that lowered the porosity [40]. The capillary pore entrance diameter significantly decreased from early to late age. The slag reaction proceeded to generate hydration products continuously filling the large pores at a late hydration age.

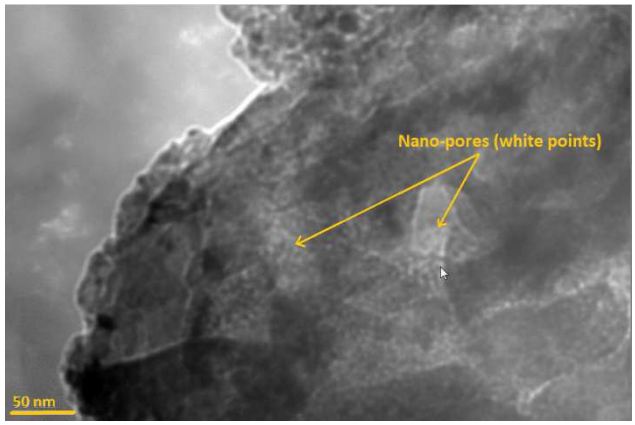

Figure 11. TEM image of $UHPC_2$ at 90 days, showing its pore structure

Figure 12 exhibits the microstructure of $UHPC_4$ cured for 3 days (left) and 90 days (right). As indicated, at 3 days, many silica fume particles do not react, and large pores can be observed, thus indicating that for lower water-to-binder ratio values, the higher the slag substitution rate, the greater the capillary pore volume. Because of the latent slag reaction at early age in the composed binder, which cured under ambient conditions, the voids and capillary pores are not efficiently filled with the limited quantity of hydration products (i.e. low density of C-S-H) previously generated at an early age. Consequently, the content of coarse pores is quite high. At 90 days, $UHPC_4$ appears with a high packing density; this result agrees with that of Yu *et al.* [43], who concluded that interparticle forces can become comparatively strong with a reduction in particle size, with as a consequence increased packing density.

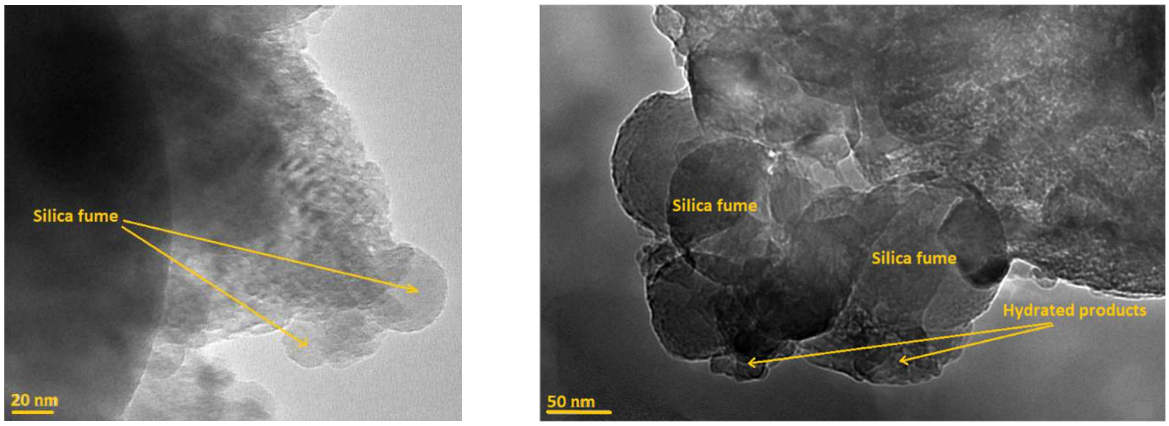

Figure 12. TEM image of UHPC$_4$ cured at 3 days (left) and 90 days (right)

It should be remarked that due to its higher specific surface area, silica fume is more susceptible to react with water than slag. This finding can be confirmed through the existence of many hydrates around silica fume particles (see Fig. 13). Many anhydrous or partially hydrated slag and silica fume particles are thus acting as fillers. From a chemical standpoint, silica fume particles act as nucleation sites, whereby hydrates emerging from the pozzolanic reaction are formed and perfectly fill the ITZ, yielding strong silica fume/hydrate bonds compared to the silica fume/quartz particle bonds (Fig. 13).

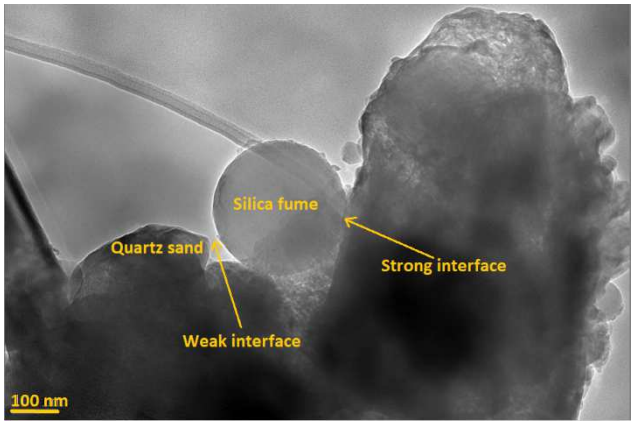

Figure 13. TEM image of UHPC$_4$ at 90 days, showing different ITZs

Figure 14 shows the low porosity of UHPC$_4$-T since the cement hydration and pozzolanic reaction have been highly activated. This observation is obvious through the pore reduction due to activation, hence density and hydration products both increase given that the heat treatment accelerates the reaction of both slag and silica fume particles. Figure 14 clearly displays the high density and high quality of the ITZ, as perfectly filled with hydrates.

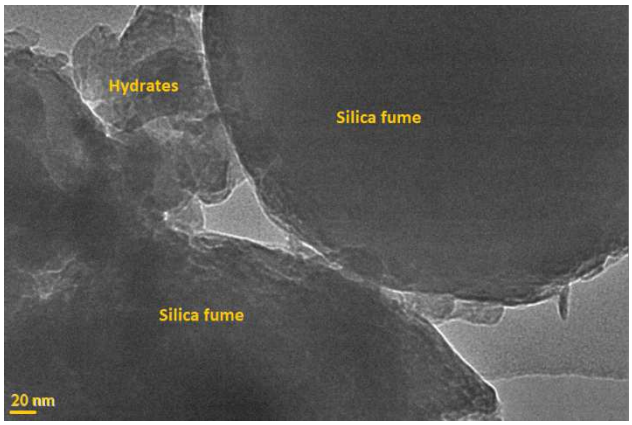

Figure 14. TEM image of UHPC4-T at 3 days

414

415 **3.3 Pore size distribution**

416 Figure 15 shows the pore size distribution curves for the various UHPCs studied at 3 days.
417 The total porosities measured are summarized in Table 3.

418 According to Figure 15, the most probable pore diameters of UHPC1 at 3 days are 0.0036 and
419 0.016 µm, indicating porous network fineness despite the early age. This result can be
420 explained by the major role played by silica fume, which decreases matrix porosity in two
421 ways:

422 - Filler impact: silica fume particles fill the voids between the cement particles themselves
423 and the spaces between cement and aggregate particles, as illustrated in the TEM image
424 (Figs. 8-9);
425 - Pozzolanic reaction: silica fume reacts with portlandite to form further C-S-H gel, as noted
426 in Figure 4 through XRD analysis and Figure 10 through the TEM image, respectively,
427 resulting in an additional decrease in both pore diameter and capillary porosity during
428 hydration progress [**44**].

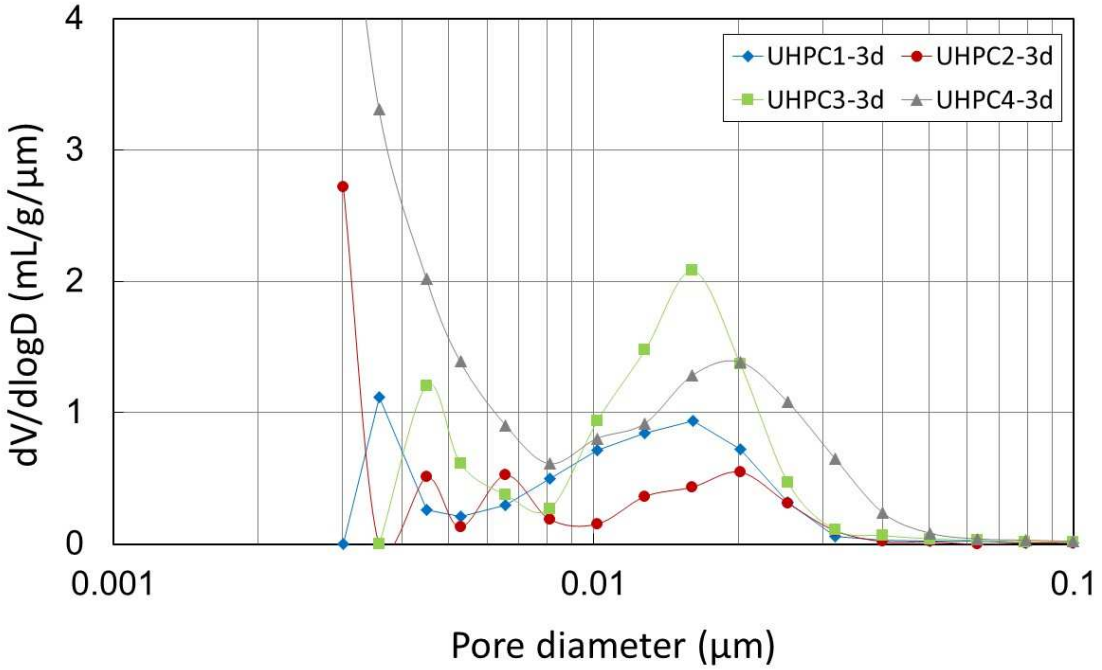

Figure 15. Incremental intrusion volume of UHPC mixtures at 3 days

Table 3: Total porosity, n (%), of investigated UHPC

Designation	$UHPC_1$	$UHPC_2$	$UHPC_3$	$UHPC_4$	$UHPC_5$	$UHPC_3$-T	$UHPC_4$-T
$n_{-3\ days}$ (%) ±0.70	5.45	4.47	10.51	12.57	7.72	2.64	4.09
$n_{-90\ days}$ (%) ±0.50	4.81	3.85	2.51	4.04	4.14	-	-

For $UHPC_2$, three pore diameter peaks are observed in Figure 15: 0.0045 µm, 0.0065 µm, and 0.0202 µm. These peaks indicate the physical role of BFS in refining the UHPC microstructure, yielding a slight decrease in porosity, compared to $UHPC_1$, despite the latent BFS reaction. At 3 days, pore diameters become large, especially in the presence of high BFS content. For $UHPC_3$, 0.0045 µm and 0.01608 µm have been measured, while for $UHPC_4$, one mean pore diameter of 0.0202 µm has been observed. Due to the latent slag reaction at an early age, the voids and capillary pores are not efficiently filled with the limited quantity of hydration products, as observed through XRD analyses for $UHPC_3$ and $UHPC_4$ in Figure 4. Consequently, the capillary pore content is high, as clearly seen in Figure 12 (left) through the TEM image for $UHPC_4$. When the pore solution pH increases, the slag begins to react with portlandite in order to generate hydration products; accordingly, the slag reaction exerts a positive impact on the pore system evolution by minimizing the critical pore size, i.e. refining porosity. Put otherwise, the critical pore diameter increases in parallel with the slag substitution rate at an early age [**21**, **45**, **46**].

At 90 days, it was indicated that the progress of the hydration reaction and the production of hydrates both filling the pores (Fig.16) and decreasing the porosity of UHPC.

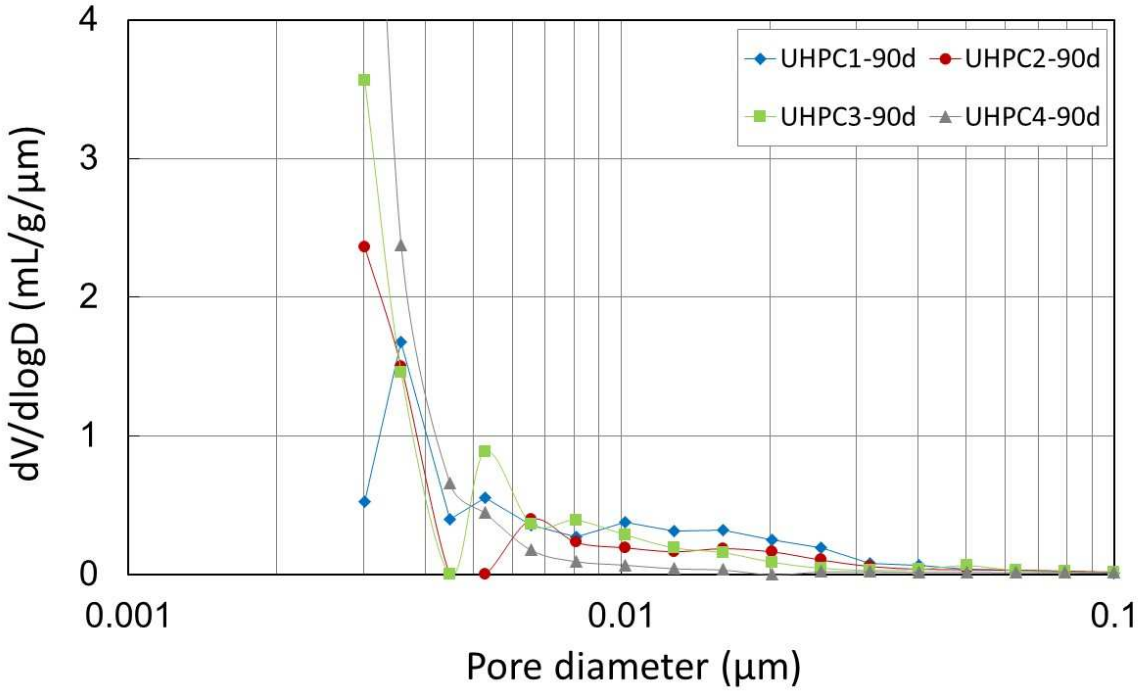

Figure 16. Incremental intrusion volume of UHPC mixtures at 90 days

From Figure 16, it was noted that the pore volume exceeding 10 nm decreases considerably, and total porosity declined for all UHPC at 90 days. $UHPC_1$ has more capillary pores (10 nm) than other UHPCs, plus two peaks of nanopores of 3.6 and 5.3 nm. The substitution of cement by 30% BFS refines the microstructure at 90 days by filling the capillary pores, so only one peak of 6.6 nm is observed. When 50% BFS is used in $UHPC_3$, this peak becomes 5.3 nm. For $UHPC_4$ (80% BFS), the capillary pores disappeared, underscoring the filling role played by BFS particles. At 90 days, the BFS particles partially react, as evident in TEM observations, hence demonstrating their physical role of filling spaces between cement particles. Furthermore, the pores are partially filled with C-S-H produced through slag hydration, resulting in a refined microstructure and decreasing total porosity [**46**, **47**]. The results obtained agreed with those from the bibliography, even though the measured total porosities were less. Cheyrezy *et al.* [**7**] tested an UHPC with a w/b ratio of 0.12; the total porosity measured was 7%, and a peak diameter of 70 nm was observed. Loukili *et al.* [**48**] demonstrated that the observed peak moves from 30 nm to 20 nm as UHPC hydration (w/b = 0.2) progresses from 1 to 7 days; they explained this observation by the pozzolanic reaction of silica fume.

Figure 17 shows the critical pore diameters for $UHPC_4$ both without and with chemical activation ($UHPC_5$).

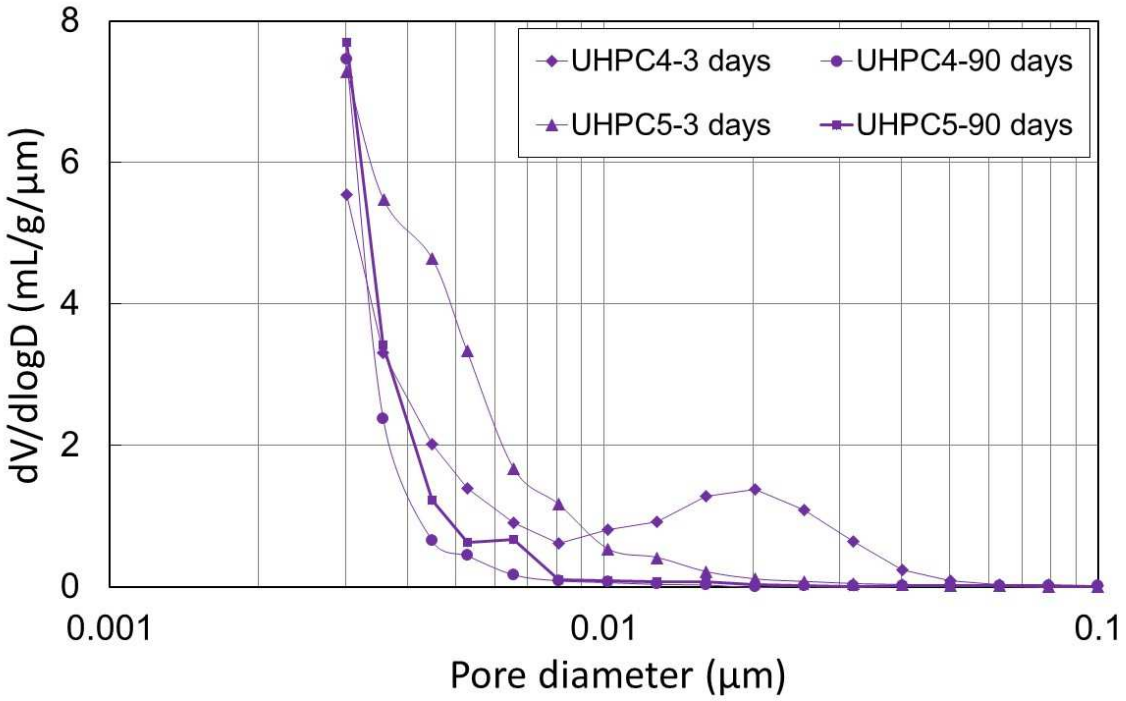

Figure 17. Incremental intrusion volume of UHPC$_4$ mixtures without and with chemical activation

As exhibited in Figure 17, adding the chemical activator causes a great reduction in capillary pores, particularly at the early age, and an increase in the volume of nano-pores. It is well known that the AAS paste is distinguished by its finer matrix system compared to that of cement paste since for the same w/b ratio, the hydration products have more gel pores and the pastes fewer capillary pores [**28**]. Several researchers have established that when a suitable chemical activator is used, the alkali-activated slag paste has less porosity, smaller pores, and the proportion of micro pores seems to be larger while the proportion of capillary pores is less than that of the Portland cement paste [**30**,**49**]. The microstructural evolution of hydrating AAS paste is governed by quick alterations at the early ages and the latent evolution later on [**28**]. This finding was discussed above using the XRD analysis presented in Figure 6.

Figure 18 shows the pore size distribution of thermally-activated mixtures (UHPC$_3$ and UHPC$_4$) respectively, compared to UHPC$_1$ at 90 days. As shown in Table 3, the measured porosities of non-activated UHPC$_3$ and UHPC$_4$ at 90 days and those thermally-activated are quite similar. Compared to UHPC$_1$, both UHPC$_3$-T and UHPC$_4$-T have fewer capillary pores and contain more nano-pores, thus denoting the beneficial effect of thermal activation in refining microstructure and decreasing porosity. These results agree with those of [**50**,**51**]. The former observed a peak of 2.5 nm for thermally-treated UHPC with a w/b ratio of 0.12, while the latter measured a 6% porosity for treated UHPC (w/c = 0.18) at 90°C.

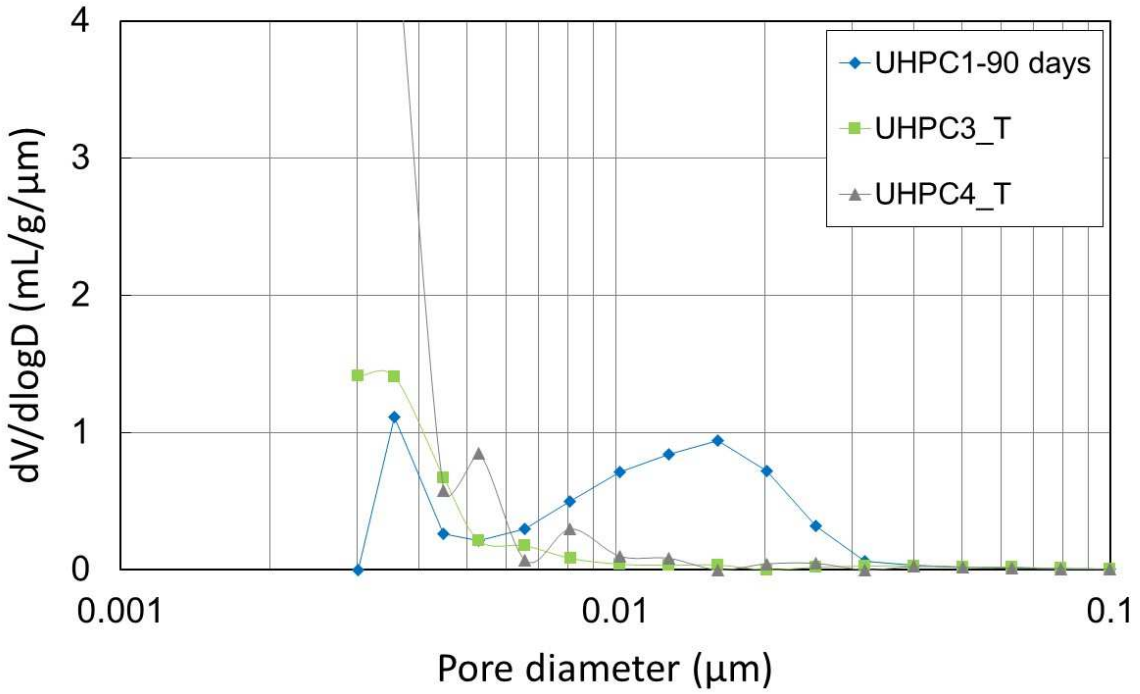

Figure 18. Incremental intrusion volume of $UHPC_1$ compared to the thermally activated mixtures of $UHPC_3$ and $UHPC_4$

3.4 Compressive strength

The use of various amounts of slag in blended UHPC mixtures yields different compressive strength values before and after applying the proposed slag activation methods. The compressive strengths of UHPC specimens with and without activation are given in Table 4.

Table 4: Compressive strength of investigated UHPC

Designation	$UHPC_1$	$UHPC_2$	$UHPC_3$	$UHPC_4$	$UHPC_5$	$UHPC_3$-T	$UHPC_4$-T
$F_{c\text{-}3\ days}$ (MPa)	110.7±3.3	113.8±2.8	82.0±1.8	37.6±0.2	53.3±2.0	164.2±4.1	134.0±5.0
$F_{c\text{-}90\ days}$ (MPa)	153.1±4.2	155.0±6.6	142.0±3.1	111.8±4.5	124.6±3.1	-	-

According to Table 4, the strength improvement ratios of $UHPC_2$ in compression are 2.8% and 1.2% for 3 and 90 days, respectively. These incremental amounts are considered as an indicator that the 30% slag replacement level exerts a positive impact on the ultimate compressive strength of $UHPC_2$. This finding is fundamentally ascribed to the greater quantity of C-S-H, which has been created in a cement/slag matrix, as sequentially observed by XRD analysis in Figures 4 and 5. The coupling effect of the high specific surface area of slag and its filling characteristics confirmed that the 30% content level performed a physical role that led to enhanced bond strength between the matrix skeleton components, as depicted in the TEM image for $UHPC_2$ in Figure 11 [**36**,**52**,**53**]. The filler impact makes reference to the

503 change in pore size distribution, as indicated in Figure 15, which can conversely be correlated
504 with mixture density.
505 It is worth noting that the slag has improved compressive strength more at 3 days than at 90
506 days. Slag substitution proved to be useful by virtue of the fact that slag shares in the
507 formation of low density C-S-H gel, as observed by the XRD analysis highlighted in Figure 5,
508 more than cement alone and gel fills the capillary pores.
509 In contrast, Table 4 reveals a loss of compressive strength in the blended UHPC specimens at
510 both ages with slag substitution levels of 50% and 80%. The drop in compressive strength of
511 $UHPC_3$ was 26% and 7%, vs. $UHPC_4$ (66%, 27%), at 3 and 90 days, respectively. These
512 internally-generated decreases are related to the chemical composition of the reaction
513 products as well as to the phase disconnection identified in the TEM images for $UHPC_4$ in
514 Figures 12 and 13, respectively [**54**,**55**]. Moreover, this finding was confirmed first through
515 XRD analysis in Figures 4 and 5, where the amount of hydrates become significantly lower
516 (especially in $UHPC_4$) by the lower portlandite content, and second in Figures 15 and 16,
517 where the pore size distribution of $UHPC_3$ and $UHPC_4$ are greatly increased at the early age
518 and then decreased at an advanced age.
519 The chemical activation served to maintain a significant rise in compressive strength, of
520 nearly 42% at 3 days, whereas at 90 days the strength gain reached approx. 14% (Table 4).
521 The dosage of activating agent is considered a paramount factor by virtue of controlling the
522 reaction rate and intensity, as well as the reaction products generated (XRD analysis, see
523 Fig.6), thus introducing an improvement effect on both early and later age performance of the
524 alkali-activated binder system [**56**]. As seen in Figure 17, the pore size distribution of $UHPC_5$
525 at 3 and 90 days confirm these results by showing an absence of critical pore size for these
526 activated mixtures at both ages.
527 Following application of the thermal activation mechanism on the $UHPC_3$ and $UHPC_4$
528 mixtures, the compressive strength results in comparison with $UHPC_1$ at 90 days, i.e. $UHPC_3$-
529 T and $UHPC_4$-T, are shown in Table 4. Compared to $UHPC_1$ at 90 days, the thermal
530 activation procedure used proved to be more appropriate in $UHPC_3$-T, whose strength grew at
531 3 days by 9%, while the 3-day strength of $UHPC_4$-T did not rise to the same extent to attain
532 an identical strength of the $UHPC_1$ at 90 days. The strength reduction of the $UHPC_4$-T
533 therefore amounted to 14%. Portlandite consumption will speed the cement reactions, which
534 in turn will consume more water, produce more portlandite and ultimately react with the silica
535 fume and slag [**57**], as observed in the TEM pore structure image of $UHPC_4$ (Fig.14). The
536 portlandite is completely consumed, due to thermal activation, in accordance with the XRD

analysis in Figure 7 for $UHPC_3$-T and $UHPC_4$-T, respectively. Moreover, the significant decrease in pore size distribution and the absence of critical $UHPC_3$-T pore diameter (Fig.18) justifies the strength improvement, compared to the reference mixture at 90 days; in contrast, let's note the presence of two peaks indicating critical $UHPC_4$-T pore diameters (Fig.18).

4. Conclusion

The following conclusions can be drawn:

- For UHPC with 30% BFS, thanks to the dual impact of a high slag specific surface area and its filling characteristics for advancing hydration and accelerating portlandite formation, the portlandite intensities are identical and the greater C-S-H quantities are closely approximated by comparison to the reference mixture ($UHPC_1$) at 3 and 90 days according to XRD analysis. As such, the pore size distribution has been refined, leading to formation of a compact microstructure, as shown through TEM images, and improved compressive strength at both ages. Accordingly, the 30% replacement level of cement by BFS can render the UHPC produced more environmentally friendly and less costly, compared to the reference ($UHPC_1$).
- For a 50% or 80% cement replacement by BFS, the portlandite intensities are lower and the peaks drop even after 3 days, as remarked through XRD analysis, hence the C-S-H intensities and unreacted alite are noticeably small for these mixtures. Thus, the capillary pores are enlarged and coarse pores increased, resulting in a reduction in compressive strength. The decrease in hydrate content was greater at 90 days. Therefore, capillary pores continue to generate, as confirmed by the TEM image of $UHPC_4$ (80% BFS), with very little change to the pore size distribution, hence the 3-day compressive strength values were slightly lower in comparative terms.
- Chemical activation by the KOH solution for the 80% BFS in $UHPC_4$ did boost BFS reactivity by providing adequate alkalis, which raised the level of portlandite consumption. Portlandite intensity thus dropped, and C-S-H amounts were further lowered at 3 and 90 days, as confirmed by XRD analysis. Dissolution of the slag glass structure and its reaction were accelerated. Consequently, the pores became smaller and compressive strength rose. Chemical activation by high doses of KOH is effective as a substitute for strength reduction.
- Thermal activation lowered the portlandite intensities in $UHPC_3$ (50% BFS) and $UHPC_4$ (80% BFS) according to XRD analysis. The pozzolanic reaction was thus highly activated due to solubility promotion by the alkali hydroxides and the large supply of portlandite released during cement hydration, leading to a decrease in pore size distribution, higher

density, a larger quantity of hydration products and ITZ quality improvements through effective filling with hydrates, as observed by the TEM image; therefore, compressive strength could be greatly improved. Consequently, thermal activation is highly efficient for developing the UHPC microstructure with high BFS content.

Acknowledgments

The corresponding author thanks Cerema and Université Gustave Eiffel for allowing the creation of the joint research team entitled "Équipe de Recherche Commune sur les Matériaux pour une Construction Durable (ERC MCD)", within which these research works were carried out.

References

[1] P. Richard, M. Cheyrezy, Composition of reactive powder concretes. Cem. Concr. Res. 25 (1995) 1501-1511.

[2] E. Fehling, M. Schmidt, J. Walraven, T. Leutbecher, S. Fröhlich, Ultra-high performance concrete UHPC: Fundamentals-Design-Examples, Wilhelm Ernst & Sohn, 10245 Berlin, Germany, 2014.

[3] M. Courtial, M.-N.D. Noirfontaine, F. Dunstetter, M.S-. Frehel, P. Mounanga, K. Cherkaoui, A. Khelidj, Effect of polycarboxylate and crushed quartz in UHPC: Microstructural investigation. Constr. Build. Mater. 44 (2013) 699-705.

[4] D. Wang, C. Shi, Z. Wu, J. Xiao, Z. Huang, Z. Fang, A review on ultra high performance concrete: Part II. Hydration, microstructure and properties. Constr. Build. Mater. 96 (2015) 368-377.

[5] J. Justs, D. Bajare, A. Korjakins, G. Mezinskis, J. Locs, G. Bumanis, Microstructural investigations of ultra-high performance concrete obtained by pressure application within the first 24 hours of hardening. Constr. Sci. 8 (2013) 50-57.

[6] C. M. Tam, V. W. Y. Tam, K. M. Ng, Optimal conditions for producing reactive powder concrete. Maga. Conc. Res. 62 (2010) 701-716.

[7] M. Cheyrezy, V. Maret, L. Frouin, Microstructural analysis of RPC (Reactive Powder Concrete). Cem. Concr. Res. 25 (1995) 1491-1500.

[8] C. Wang, C. Yang, F. Liu, C. Wan, X. Pu, Preparation of ultra-high performance concrete with common technology and materials. Cem. Concr. Comp. 34 (2012) 538-544.

[9] C. Shi, Z. Wu, J. Xiao, D. Wang, Z. Huang, Z. Fang, A review on ultra high performance concrete: part I. raw materials and mixture design. Constr. Build. Mater. 101 (2015) 741-751.

603 [10] M. K. Maroliya, A qualitative study of reactive powder concrete using X-ray diffraction
604 technique. IOSR. Jour. Eng. 2 (9) (2012) 12-16.
605 [11] T. Oertel, U. Helbig, F. Hutter, H. Kletti, G. Sextl, Influence of amorphous silica on the
606 hydration in ultra-high performance concrete. Cem. Concr. Res. 58 (2014) 121-130.
607 [12] A. Cwirzen, V. Penttala, C. Vornanen, Reactive powder based concretes: Mechanical
608 properties, durability and hybrid use with OPC. Cem. Concr. Res. 38 (2008) 1217-1226.
609 [13] P. Hájek, C. Fiala, Environmentally optimized floor slabs using UHPC- contribution to
610 sustainable construction. Proceedings of the 2nd International Symposium on Ultra High
611 Performance Concrete, Kassel, Germany, 2008, pp.879-886.
612 [14] H. Kim, T. Koh, S. Pyo, Enhancing flowability and sustainability of ultra high
613 performance concrete incorporating high replacement levels of industrial slags. Constr. Build.
614 Mater. 123 (2016) 153-160.
615 [15] G. Xu, Q. Tian, J. Miao, J. Liu, Early-age hydration and mechanical properties of high
616 volume slag and fly ash concrete at different curing temperatures. Constr. Build. Mater. 149
617 (2017) 367-377.
618 [16] S. Gupta, Effect of content and fineness of slag as high volume cement replacement on
619 strength and durability of ultra-high performance mortar. J. Build. Mater. Struct. 3 (2016) 43-
620 54.
621 [17] J.F. Lamond, J.H. Pielert, Significance of tests and properties of concrete and concrete-
622 making materials, ASTM International, West Conshohocken, PA, ASTM Stock No.:
623 STP169D, 2006.
624 [18] C. C. Castellano, V. L. Bonavetti, H. A. Donza, E.F. Irassar, The effect of w/b and
625 temperature on the hydration and strength of blastfurnace slag cements. Constr. Build. Mater.
626 111 (2016) 679-688.
627 [19] A. M. Rashad, An investigation on very high volume slag pastes subjected to elevated
628 temperatures. Constr. Build. Mater. 74 (2015) 249-258.
629 [20] F. Bellmann, J. Stark, Activation of blast furnace slag by a new method. Cem. Concr.
630 Res. 39 (2009) 644-650.
631 [21] J. Zhou, G. Ye, K. van Breugel, Hydration process and pore structure of portland cement
632 paste blended with blast furnace slag. Proceedings of the 6th International Symposium on
633 Cement & Concrete and Canmet, 2006, pp.1-7.
634 [22] R. Taylor, I.G. Richardson, R.M.D. Brydson, Composition and microstructure of 20-
635 year-old ordinary Portland cement–ground granulated blast-furnace slag blends containing 0
636 to 100% slag. Cem. Concr. Res. 40 (2010) 971-983.

637 [23] A. Hadj-sadok, S. Kenai, L. Courard, A. Darimont, Microstructure and durability of
638 mortars modified with medium active blast furnace slag. Constr. Build. Mat. 25 (2011) 1018-
639 1025.
640 [24] M. Bertin, O.O. Metalssi, V.B. Bouny, M. Saillio, Changes in microstructure and pore
641 structure of low-clinker cementitious materials during early stages of carbonation.
642 Proceedings of the 2nd International Conference in Concrete Sustainability (ICCS 16),
643 Madrid, Spain, 2016, pp.1-12.
644 [25] K.V. Schuldyakova, L.Y. Kramara, B.Y. Trofimov, The properties of slag cement and its
645 influence on the structure of the hardened cement paste. Proc. Eng. 150 (2016) 1433-1439.
646 [26] A. Bougara, C. Lynsdale, K. Ezziane, Activation of Algerian slag in mortars. Constr.
647 Build. Mater. 23 (2009) 542-547.
648 [27] A. Wetzel, B. Middendorf, Influence of silica fume on properties of fresh and hardened
649 ultra-high performance concrete based on alkali-activated slag. Cem. Concr. Compos. 100
650 (2019) 53–59.
651 [28] W. Chen, Hydration of slag cement: Theory, modeling, and application, University of
652 Twente, The Netherlands, Doctoral Thesis, 2007.
653 [29] S. Aydın, B. Baradan, Effect of activator type and content on properties of alkali-
654 activated slag mortars. Comp. Par. B. 57 (2014) 166-172.
655 [30] C. Shi, P.V. Krivenko, D. Roy, Alkali-activated cements and concretes, 1st Edition,
656 Taylor & Francis group, 2006.
657 [31] R. J. Thomas, H. Ye, A. Radlińska, S. Peethamparan, Alkali-activated slag cement
658 concrete: A closer look at a sustainable alternative to portland cement. Concr. Intern. 38 (1)
659 (2016) 33-38.
660 [32] M.A. Abd-El.Aziz, S. Abd.El.Aleem, M. Heikal, Physico-chemical and mechanical
661 characteristics of pozzolanic cement pastes and mortars hydrated at different curing
662 temperatures. Const. Build. Mater. 26 (2012) 310-316.
663 [33] C.-M. Aldea, F. Young, K. Wang, S.P. Shah, Effects of curing conditions on properties
664 of concrete using slag replacement. Cem. Concr. Res. 30 (2000) 465-472.
665 [34] O. M. Abdulkareem, A. Ben Fraj, M. Bouasker, A. Khelidj, Mixture design and early age
666 investigations of more sustainable UHPC. Const. Build. Mater. 163 (2018) 235-246.
667 [35] P. Mounanga, M.I. Ahmad Khokhar, R. El Hachem, A. Loukili, Improvement of the
668 early-age reactivity of fly ash and blast furnace slag cementitious systems using limestone
669 filler. Mater. Struct. 44 (2011) 437-453.

[36] O. M. Abdulkareem, A. Ben Fraj, M. Bouasker, A. Khelidj, Effect of chemical and thermal activation on the microstructural and mechanical performance of more sustainable UHPC. Const. Build. Mater. 169 (2018) 567-577.
[37] NF EN 196-1: Methods of testing cement - Part 1: determination of strengths, 2016, French Standard.
[38] O.M. Abdulkareem, A. Ben Fraj, M. Bouasker, A. Khelidj, Early age and mechanical properties of environmentally friendly ultra high performance concrete. Proceedings of the 9th International Concrete Conference: Environment, Efficiency, and Economic Challenges for Concrete, Dundee, Scotland, 2016, pp.827-838.
[39] M. Ashraf, A.N. Khan, Q. Ali, J. Mirza, A. Goyal, A.M. Anwar, Physico-chemical, morphological and thermal analysis for the combined pozzolanic activities of minerals additives. Const. Build. Mater. 23 (2009) 2207-2213.
[40] V. Kocaba, Development and evaluation of methods to follow microstructural development of cementitious systems including slags, École Polytechnique Fédérale of Lausanne, Switzerland, Doctoral Thesis, 2009.
[41] M. Ben Haha, G. Le Saout, F. Winnefeld, B. Lothenbach, Influence of activator type on hydration kinetics, hydrate assemblage and microstructural development of alkali activated blast-furnace slags. Cem. Concr. Res. 41 (2011) 301-310.
[42] L. Gatty, S. Bonnamy, A. Feylessoufi, C. Clinard, P. Richard, H. Van Damme, A transmission electron microscopy study of interfaces and matrix homogeneity in ultra-high-performance cement-based materials. Jour. Mater. Sci. 36 (2001) 4013-4026.
[43] I. Mehdipour, K. H. Khayat, Effect of particle-size distribution and specific surface area of different binder systems on packing density and flow characteristics of cement paste. Cem. Concr. Compos. 78 (2017) 120-131.
[44] C. Shi, D. Wang, L. Wu, Z. Wu, The hydration and microstructure of ultra high-strength concrete with cement-silica fume-slag binder. Cem. Concr. Comp. 61 (2015) 44-52.
[45] E. Berodier, K. Scrivener, Evolution of pore structure in blended systems. Cem. Concr. Res. 73 (2015) 25-35.
[46] L. Rengguang, D. Shidong, Y. Peiyu, Microstructure of hardened complex binder pastes blended with slag. Jour. Chin. Cera. Soc. 43 (5) (2015) 610-618.
[47] A. A. Ramezannianpour, Cement Replacement Materials: Properties, Durability, Sustainability, Springer-Verlag Berlin Heidelberg, Germany, 2014.

[48] A. Loukili, A. Khelidj, P. Richard, Hydration kinetics, change of relative humidity, and autogenous shrinkage of ultra-high-strength concrete. Cem. Concr. Res. 29 (4) (1999) 577-584.
[49] F. Collinsa, J.G. Sanjayan, Effect of pore size distribution on drying shrinkage of alkali-activated slag concrete. Cem. Concr. Res. 30 (2000) 1401-1406.
[50] A. Feylessoufi, F. Villiéras, L.J. Michot, P. De Donato, J.M. Cases, P. Richard, Water, environmental, and nano-structural network in a reactive powder concrete. Cem. Concr. Compos. 18 (1) (1996) 23-29.
[51] V. Matte, Durability of ultra high performance concrete: Role of cementitious matrix, ENS Cachan University of Sherbrooke, Canada, Doctoral Thesis, 1999.
[52] H. Yazıcı, M.Y. Yardımcı, S. Aydın, A.S. Karabulut, Mechanical properties of reactive powder concrete containing mineral admixtures under different curing regimes. Constr. Build. Mater. 23 (2009) 1223-1231.
[53] R. Siddique, Waste Materials and By-Products in Concrete, Springer-Verlag Berlin Heidelberg, 2008.
[54] F. Sajedi, H. Abdul Razak, Effects of thermal and mechanical activation methods on compressive strength of ordinary Portland cement–slag mortar. Mater. and. Des. 32 (2011) 984-995.
[55] O. Kayali, J.M. Khatib, M.S. Ahmed, The role of industrial by-products in creating sustainable concrete. International Seminar: Innovation & valorization in civil engineering & construction materials, No. 1O-304, Morocco, 2011.
[56] M. Heikal, M.Y. Nassar, G. El-Sayed, S.M. Ibrahim, Physico-chemical, mechanical, microstructure and durability characteristics of alkali activated Egyptian slag. Constr. Build. Mater. 69 (2014) 60-72.
[57] H. Yazıcı, M.Y. Yardımcı, H. Yiğiter, S. Aydın, S. Türkel, Mechanical properties of reactive powder concrete containing high volumes of ground granulated blast furnace slag. Cem. Concr. Compos. 32 (2010) 639-648.